Multicolor coherence-induced negative refraction in three-level atomic system

Hongju Guo (郭洪菊)[1], Hongjun Zhang (张红军)[1,2*], Chunfang Wang (王春芳)[3], and Yu Chen (陈 昱)[1]

[1] *Shanghai Publishing and Printing College, Shanghai 200093, China*

[2] *College of Physics and Information Technology, Shaanxi Normal University, Xi'an 710062, China*

[3] *School of Science, University of Shanghai for Science and Technology, Shanghai 200093, China*

[*] *Corresponding author: zhhjun@snnu.edu.cn*

Received July 6, 2012; accepted August 7, 2012; posted online September 26, 2012

Multicolor manipulation of negative refraction in a three-level Λ atomic system is theoretically investigated. Based on multicolor coherence, the negative refractive index can be obtained with reduced absorption. The refractive index can also be controlled by changing the sum of the phases of the sidebands in the trichromatic driving fields. By adjusting the sum phase, the refractive index can be varied between negative and positive in two different frequency bands. Furthermore, the frequency band corresponding to the negative refractive index is widened by increasing the intensity and the frequency difference of the trichromatic field.

OCIS codes: 270.1670, 190.4400, 160.4330.

doi: 10.3788/COL201210.122701.

The left-handed material (LHM)[1] has recently been widely investigated because of its counterintuitive properties. In these materials, the inverse Snell law, reverse Cerenkov effect, and reverse Doppler shift can appear. With the remarkable properties of negative refraction, including amplification of evanescent waves[2,3] and photon tunneling[4], LHM can be used to focus all Fourier components of a two-dimensional image as a perfect lens[5]. LHM is not available in nature: it is artificially manufactured[6−12] by delicately constructing spatial periodic structures[13,14]. Recently, schemes based on quantum coherence and interference have been put forward simultaneously by Oktel *et al.*[15,16] to achieve negative refraction in a three-level medium. However, in these examples, absorption reduces the resolution of a perfect lens[17]. Numerous proposals have been put forward to reduce absorption[18−22]. Thommen *et al.* proposed a four-level scheme in which an electric (magnetic) atomic transition was used as an electric (magnetic) resonator to modify the permittivity (permeability), and at the same frequency, to electromagnetically induce left-handed properties[18]. Kastel *et al.* presented a five-level scheme based on electromagnetically induced chirality, which can achieve negative refractive index without absorption[20].

However, all of the above are examples of materials interacting with monochromatic optical fields. A monochromatic field with a single frequency value exists only in ideal states. By contrast, a multicolor field, a resonant optical field with sidebands, is considered closer to reality. Multicolor coherence in the atomic system could induce many interesting phenomena[23,24], and manipulate the absorptive and dispersive properties[25,26]. In this letter, we study the negative refraction based on multicolor coherence, where a three-level Λ atomic gas system is coupled with a strong trichromatic driving field and a weak monochromatic probe field. By accurately tuning the frequency difference and three Rabi frequencies of the trichromatic driving field, the negative refraction with reduced absorption can appear resulting from the quantum interference between multi-interaction paths. By considering phase influence in this system, the refractive index is found to depend on the sum of the relative phases of the sideband components. Adjusting the sum phase, the refractive index can be altered between negative and positive in two different frequency bands. In addition, the frequency band corresponding to the negative refraction can be widened by increasing the intensity and the frequency difference of the trichromatic field.

We consider a three-level Λ-type system as shown in Fig. 1[15], which includes an excited state and two lower states, signed by $|0\rangle$, $|1\rangle$, and $|2\rangle$, respectively. Two lower states, $|1\rangle$ and $|2\rangle$ have the same parity with $\vec{\mu}_{21} = \langle 2|\,\hat{\vec{\mu}}\,|1\rangle \neq 0$, where $\hat{\vec{\mu}}$ is the magnetic dipole operator. The upper state $|0\rangle$ has an opposite parity to the lower states $|1\rangle$ and $|2\rangle$ with $\vec{d}_{10} = \langle 1|\,\hat{\vec{d}}\,|0\rangle \neq 0$ and $\vec{d}_{20} = \langle 2|\,\hat{\vec{d}}\,|0\rangle \neq 0$, where $\hat{\vec{d}}$ is the electric dipole operator. The $|0\rangle \rightarrow |2\rangle$ transition is coupled with a trichromatic driving field $(\vec{E}_0 + \vec{E}_1 e^{\mathrm{i}\delta t} + \vec{E}_2 e^{-\mathrm{i}\delta t})e^{-\mathrm{i}\omega_0 t} + c.c.$, and the $|0\rangle \rightarrow |1\rangle$ transition is coupled with a weak monochromatic probe field $\vec{E}_{\mathrm{p}} e^{-\mathrm{i}\omega_p t} + c.c.$, in which $\vec{E}_i (i = 0 - 2, \mathrm{p})$ are the field amplitudes of each components of the driving and probe fields, ω_0 is the central frequency of the driving field, ω_{p} is the probe frequency, and δ is the frequency difference among the three components of the driving field. $\Delta_{\mathrm{p}} = \omega_{01} - \omega_{\mathrm{p}}$ and $\Delta_{\mathrm{d}} = \omega_{02} - \omega_0$ are the detunings of the respective fields from the corresponding transitions. γ_1, γ_2, and γ_3 are the spontaneous emission decay rates respectively corresponding to the $|0\rangle \rightarrow |1\rangle$, $|0\rangle \rightarrow |2\rangle$,and $|1\rangle \rightarrow |2\rangle$ transitions. $\Omega_i = \frac{\vec{d}_{20} \cdot \vec{E}_i}{\hbar} (i = 0 - 2)$ and $\Omega_{\mathrm{p}} = \frac{\vec{d}_{10} \cdot \vec{E}_{\mathrm{p}}}{\hbar}$ represent Rabi frequencies related to the respective fields. In general, we set the Rabi frequencies Ω_0, Ω_{p} to be real. Hence we take $\Omega_j =$

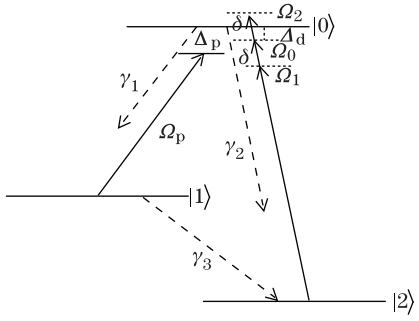

Fig. 1. Scheme of a three-level Λ atomic system interacting with a monochromatic probe field and a trichromatic driving field.

$|\Omega_j|\, e^{-i\phi_j} (j = 1, 2)$, where $\phi_{1,2}$ are the relative phases of the sideband components $\vec{E}_{1,2}$ of the trichromatic driving field with respect to that of the central component $\vec{E}_0$. The sum of the relative phases $\phi_{1,2}$ is defined as $\Phi = \phi_1 + \phi_2$. The magnetic interaction strengths are typically two orders of magnitude smaller than the electric interaction strengths. Without loss of generality, we neglected it in the following calculation[15,18]. By using the rotating-wave approximation, the equations of density matrix elements are derived as

$$\begin{cases} \dot{\rho}_{00} = -(\gamma_1+\gamma_2)\rho_{00} + \frac{i\Omega_p}{2}\rho_{10} - \frac{i\Omega_p^*}{2}\rho_{01} + \frac{iG}{2}\rho_{20} - \frac{iG^*}{2}\rho_{02} \\ \dot{\rho}_{11} = \gamma_1\rho_{00} - \gamma_3\rho_{11} - \frac{i\Omega_p}{2}\rho_{10} + \frac{i\Omega_p^*}{2}\rho_{01} \\ \dot{\rho}_{22} = \gamma_2\rho_{00} + \gamma_3\rho_{11} - \frac{iG}{2}\rho_{20} + \frac{iG^*}{2}\rho_{02} \\ \dot{\rho}_{01} = -(\frac{\gamma_1+\gamma_2+\gamma_3}{2} + i\Delta_p)\rho_{01} - \frac{i\Omega_p}{2}\rho_{00} + \frac{i\Omega_p}{2}\rho_{11} + \frac{iG}{2}\rho_{21} \\ \dot{\rho}_{02} = -(\frac{\gamma_1+\gamma_2}{2} + i\Delta_d)\rho_{02} + \frac{i\Omega_p}{2}\rho_{12} + \frac{iG}{2}(1 - \rho_{11} - 2\rho_{00}) \\ \dot{\rho}_{21} = [i(\Delta_d - \Delta_p) + \frac{\gamma_3}{2}]\rho_{21} - \frac{i\Omega_p}{2}\rho_{20} + \frac{iG^*}{2}\rho_{01}. \end{cases} \quad (1)$$

Equation (1) is constrained by $\rho_{00} + \rho_{11} + \rho_{22} = 1$ and $\rho_{ij}^* = \rho_{ji}$. We thus set $G = (\Omega_0 + \Omega_1 e^{i\delta t} + \Omega_2 e^{-i\delta t})$ and $G^* = (\Omega_0^* + \Omega_1^* e^{-i\delta t} + \Omega_2^* e^{i\delta t})$. For the purpose of solving Eq. (1), we expand the density matrix elements in a Fourier series as

$$\rho_{jk} = \sum_{n=-\infty}^{+\infty} \rho_{jk}^{(n)} e^{in\delta t} \ (j, k = 0, 1, 2). \quad (2)$$

Substituting Eq. (2) into Eq. (1), we obtain the inverse matrix[26,27] and the steady solution for the column vector

$$\begin{aligned} \vec{X} = (&\rho_{01}^{(-L)}, \rho_{10}^{(-L)}, \rho_{02}^{(-L)}, \rho_{20}^{(-L)}, \rho_{21}^{(-L)}, \rho_{12}^{(-L)}, \rho_{11}^{(-L)}, \\ &\rho_{00}^{(-L)}, \rho_{01}^{(-L+1)}, \cdots, \rho_{00}^{(-L+1)}, \\ &\cdots, \rho_{01}^{(0)}, \cdots, \rho_{00}^{(0)}, \cdots, \rho_{01}^{(L-1)}, \\ &\cdots, \rho_{00}^{(L-1)}, \cdots, \rho_{01}^{(L)}, \cdots, \rho_{00}^{(L)})^{\mathrm{T}}, \end{aligned}$$

where L is a natural number. In our numerical calculation, $L = 15$ is chosen to meet accuracy.

Next, we discuss the electric and magnetic responses of the medium to the probe field. In Eq. (2), the zero order components of the coherence terms play an important role in response to the probe field because they merely oscillate with the probe field[27]. Thus, the complex electric dipole moment of the medium is given by $\vec{p}(\omega_p) = \vec{d}_{10}\rho_{01}^{(0)}$ based on quantum theory[15,26]. Moreover, the complex atomic polarizability tensor α_e can be described as $\vec{p}(\omega_p) = \varepsilon_0\alpha_e(\omega_p)\vec{E}_p(\omega_p)$, in which $\vec{E}_p$ is chosen to be parallel to atomic dipole $\vec{d}_{10}$ so that α_p is a scalar. Thus, the electric polarizability for the probe field is expressed as

$$\alpha_e = \frac{d_{10}\rho_{01}^{(0)}}{\varepsilon_0 E_p} = \frac{|d_{10}|^2 \rho_{01}^{(0)}}{\varepsilon_0 \hbar \Omega_p}. \quad (3)$$

Similarly, the magnetic response of the medium to the probe field is associated with the coherent term $\rho_{21}^{(0)}$, and the atomic magnetizability can be obtained as[28]

$$\alpha_m = \frac{\mu_0 c \mu_{12} \rho_{21}^{(0)}}{\eta E_p}, \quad (4)$$

where c is the speed of light in vacuum, μ_0 is the permeability of vacuum, and η is a unitary complex number depending on the polarization of the probe field $\vec{E}_p$.

Using Eqs. (3) and (4), the relative permittivity and the relative permeability are easily obtained[18]

$$\varepsilon_r = 1 + N\alpha_e, \quad (5)$$

$$\mu_r = \frac{1}{1 - N\alpha_m}, \quad (6)$$

where N is the atomic density.
For LHM, the refractive index is defined as[1]

$$n_r = -\sqrt{\varepsilon_r \mu_r}. \quad (7)$$

The strong magnetic response of the probe field to the medium is obtained by setting the induced magnetic dipole transition to oscillate in phase with the probe beam and constraining the three-level system as $\omega_{02} = 2\omega_{01}$[15].

We then consider a gas of ^{23}Na atoms with $N = 10^{22}$ m^{-3} and study the negative refractive property of this atomic system on the basis of multicolor quantum coherence. The electric and magnetic polarizabilities for atoms are chosen as $d_{01} = 8.5 \times 10^{-30}$C·m and $\mu_{21} = 6.4 \times 10^{-23}$C·m^2 · s^{-1}($\approx d_{01}c\alpha/2$ with the fine structure constant $\alpha = \frac{1}{137}$)[29]. In numerical calculations, the spontaneous emission rate is estimated to be $\gamma_1 \sim 10.06$ MHz by using the relation $d_{10} = \sqrt{3\gamma_1\hbar\varepsilon_0\lambda^3/8\pi^2}$, in which $\lambda \sim 589$ nm is the wavelength of the resonant probe transition. Other parameters are simplified as dimensionless by scaling with $\gamma = \gamma_1$, and typical values of $\gamma_2 = 0.5\gamma$, $\gamma_3 = 6 \times 10^{-4}\gamma$, $\Omega_p = 0.001\gamma$, and Δ_d=0 are used. For different values of three Rabi frequencies of the driving field (Ω_0, Ω_1, Ω_2), the corresponding frequency difference δ and the sum phase Φ, the frequency dependence of the real part of the

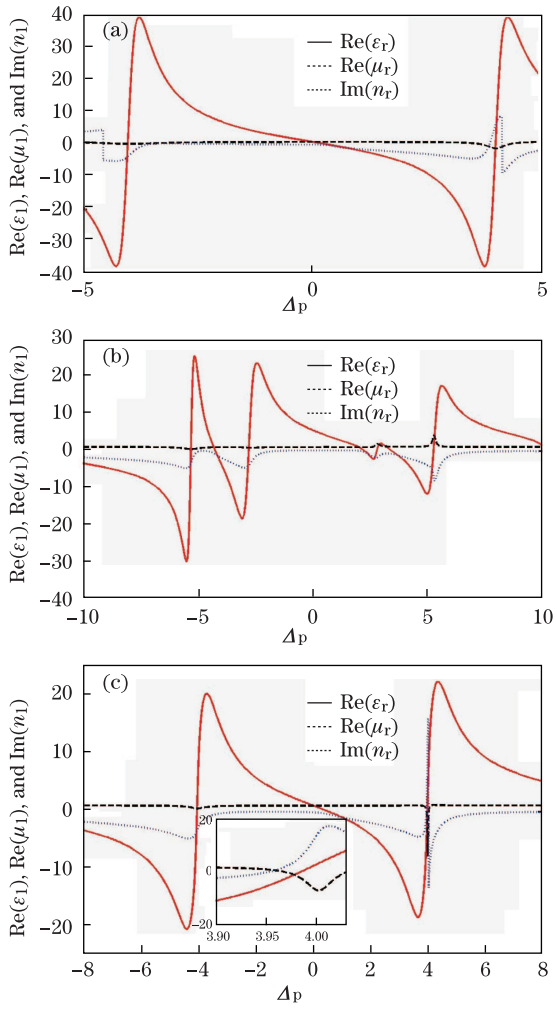

Fig. 2. Frequency dependence of the relative dielectric permittivity ε_r, the relative magnetic permeability μ_r and the refractive index n_r of three-level atoms with Φ=0, and (a) $\Omega_0 = 8\gamma$, $\Omega_1 = \Omega_2 = \delta$=0; (b) Ω_0=$\Omega_1 = \delta = 8\gamma$, Ω_2=0; (c) Ω_0=$\Omega_1 = \Omega_2 = \delta = 8\gamma$.

relative electric permittivity ε_r and magnetic permeability μ_r, along with the imaginary part of the refractive index n_r, are drawn in Figs. 2 to 4.

Under the condition $\Phi = 0$, we plot the real part of ε_r (Re[ε_r], solid line), the real part of μ_r (Re[μ_r], dashed line) as well as the imaginary part of refractive index n_r (Im[n_r], dotted line) versus the probe detuning in Fig. 2. We then investigate the negative refractive property for the cases of monochromatic, dichromatic and trichromatic driving field. When the driving field is monochromatic, the real part of magnetic permeability presents very small negative values in the right frequency band as exhibited in Fig. 2(a). With the driving filed being replaced by a dichromatic field, the curves about Re[ε_r], Re[μ_r] and Im[n_r] change significantly, as shown in Fig. 2(b). Four peaks appear for the real part of magnetic permeability, and the gain is maintained for all frequency bands. However, the real part of magnetic permeability is always positive, which indicates that the negative refractive phenomenon is very weak or does not appear for the monochromatic and dichromatic driving field under the given parameters. However, when the driving field is adjusted to be trichromatic, the permittivity and the permeability are simultaneously negative in the area of $3.954\gamma < \Delta_p < 3.990\gamma$, thereby corresponding to frequency bandwidth of $\sim$ 0.36 MHz as demonstrated in Fig. 2(c). Furthermore, in this negative refraction frequency band, the imaginary part of refractive index n_r related to the absorption is reduced, as indicated in the insert in Fig. 2(c). This condition is suitable for application. The interference between multi-interaction paths of trichromatic coherence makes it possible to achieve negative refraction in a wide frequency band.

Phase dependence also plays a key role in multicolor coherent effects. We turn to consider the phase influence of the negative refraction in this system. Adjusting the sum phase to be $\Phi = \pi$ with other parameters being the same as in Fig. 2(c), we plot the probe-detuning dependence of the real part of ε_r (solid line), the real part of μ_r (dashed line), and the imaginary part of refractive index n_r (dotted line) in Fig. 3. Comparing Fig. 3 with Fig. 2(c), we find the negative refractive property depends strongly on the sum phase. Altering the sum phase from 0 to π, the structure of peaks about electric permittivity and magnetic permeability are changed significantly. The frequency band corresponding to both negative permittivity and negative permeability is shifted to $7.756\gamma < \Delta_p < 7.848\gamma$, and widened to be $\sim$ 0.93 MHz, as described in the enlarged figure (inserted in Fig. 3), which is approximately three times that of Fig. 2(c). However, Fig. 3 shows that in the same negative refractive frequency band corresponding to $\Phi = 0$, the electric permittivity and magnetic permeability simultaneously become positive. Thus, refractive index can be switched between negative and positive in two different frequency bands by adjusting the sum phase[30], which can provide a convenient way to transform the refractive nature of the medium in practical application.

Additionally, we consider the effect of the intensity of the trichromatic field and the frequency difference (Ω_0, Ω_1, Ω_2, δ) on the properties of electric permittivity and magnetic permeability in Fig. 4. By comparing Figs. 4(a) and (b) with Fig. 2(c), we find that simul-

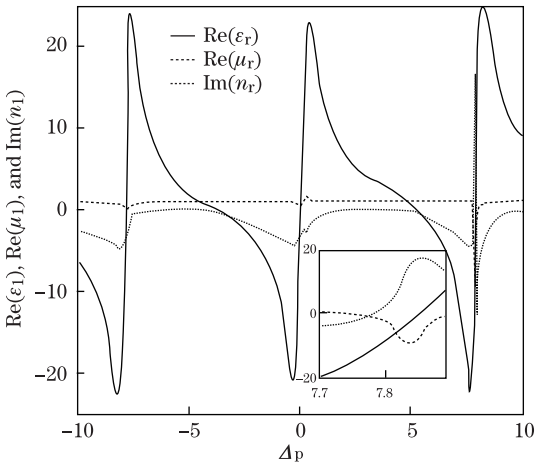

Fig. 3. Real parts of ε_r and μ_r, along with the imaginary of n_r versus frequency detuning Δ_p for the case of $\Phi = \pi$ and $\Omega_0 = \Omega_1 = \Omega_2 = \delta = 8\gamma$.

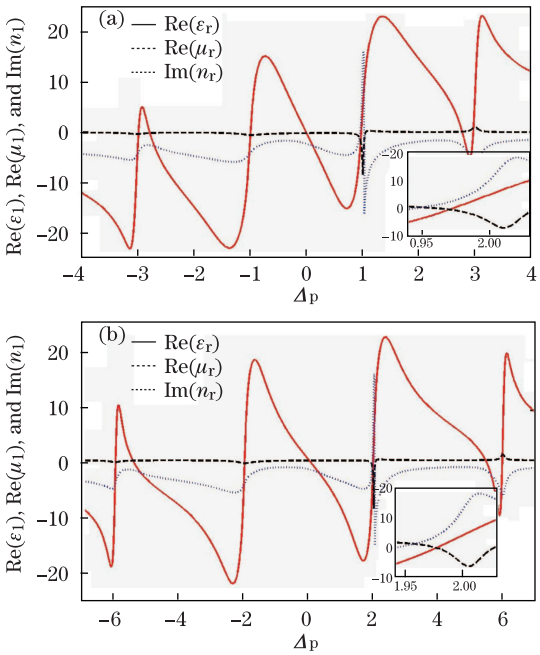

Fig. 4. Frequency dependence of the real electric permittivity ε_r and magnetic permeability μ_r, along with the imaginary of n_r for (a) $\Omega_0 = \Omega_1 = \Omega_2 = \delta = 2\gamma$, and (b) $\Omega_0 = \Omega_1 = \Omega_2 = \delta = 4\gamma$.

taneously increasing the intensity of trichromatic field and the frequency difference $\Omega_0 = \Omega_1 = \Omega_2 = \delta$ can widen the frequency band corresponding to the negative refractive index from 0.32 to 0.34 and 0.36 MHz. The increased negative refractive frequency band has a favorable and practical use for operating.

In conclusion, we study multicolor coherence-induced negative refractive index in a three-level Λ type atomic configuration. Based on trichromatic coherence, negative refraction with reduced absorption is achieved. The sum of the relative phases of the sideband components also plays a crucial role in the properties of electric permittivity and magnetic permeability. Negative refraction can be obtained in a different frequency band by changing the sum phase from 0 to π. The refractive index can be switched between negative and positive by controlling the sum phase in two different frequency bands. Gradually increasing the intensity of the trichromatic field and the frequency difference between the driving field components can further widen the frequency band corresponding to the negative refraction.

References

1. V. G. Veselago, Sov. Phys. Usp. **10,** 509 (1968).
2. J. B. Pendry, Phys. Rev. Lett. **85,** 3966 (2000).
3. L. Chen, S. He, and L. Shen, Phys. Rev. Lett. **92,** 107404 (2004).
4. Z. M. Zhang and C. J. Fu, Appl. Phys. Lett. **80,** 1097 (2002).
5. G. W.'t Hooft, Phys. Rev. Lett. **87,** 249701 (2001).
6. R. A. Shelby, D. R. Smith, and S. Schultz, Science **292,** 77 (2001).
7. J. Pendry, Nature **423,** 22 (2003).
8. C. G. Parazzoli, R. B. Greegor, K. Li, B. E. C. Koltenbah, and M. Tanielian, Phys. Rev. Lett. **90,** 107401 (2003).
9. J. B. Pendry, A. J. Holden, D. J. Robbins, and W. J. Stewart, J. Phys. **10,** 4785 (1998).
10. J. B. Pendry, A. J. Holden, W. J. Stewart, and I. Youngs, Phys. Rev. Lett. **76,** 4773 (1996).
11. S. P. Burgos, R. de Waele, A. Polman, and H. A. Atwater, Nat. Mater. **9,** 407 (2010).
12. S. Palomba, S. Zhang, Y. Park, X. Yin, and X. Zhang, Nat. Mater. **11,** 34 (2012).
13. A. Berrier, M. Mulot, M. Swillo, M. Qiu, L. Thylén, A. Talneau, and S. Anand, Phys. Rev. Lett. **93,** 073902 (2004).
14. S. He, Z. Ruan, L. Chen, and J. Shen, Phys. Rev. B **70,** 115113 (2004).
15. M. Ö. Oktel and Ö. E. Müstecaplioğu, Phys. Rev. A **70,** 053806 (2004).
16. J. Q. Shen, Z. C. Ruan, and S. He, J. Zhejiang Univ. Science (in Chinese) **5,** 1322 (2004).
17. S. A. Ramakrishna, Rep. Prog. Phys. **68,** 449 (2005).
18. Q. Thommen and P. Mandel, Phys. Rev. Lett. **96,** 053601 (2006).
19. H. Zhang, Y. Niu, and S. Gong, Phys. Lett. A **363,** 497 (2007).
20. J. Kastel, M. Fleischhauer, S. F. Yelin, and R. L. Walsworth, Phys. Rev. Lett. **99,** 073602 (2007).
21. A. R. Katko, S. Gu, J. P. Barrett, B. I. Popa, G. Shvets, and S. A. Cummer, Phys. Rev. Lett. **105,** 123905 (2010).
22. H. Zhang, Y. Niu, H. Sun, and S. Gong, Chin. Opt. Lett. **6,** 373 (2008).
23. X. M. Hu, Q. Xu, J. Y. Li, X. X. Li, W. X. Shi, and X. Zhang, Opt. Commun. **260,** 196 (2006).
24. J. P. Zhang, J. Xu, G. Hernandez, X. M. Hu, and Y. F. Zhu, Phys. Rev. A **75,** 043810 (2007).
25. Z. Ficek, J. Seke, A. V. Soldatov, G. Adam, and N. N. Bogolubov, Opt. Commun. **217,** 299 (2003).
26. H. J. Guo, X. M. Hu, J. Y. Li, X. X. Li, W. X. Shi, and Q. Xu, Chin. Phys. **15,** 0383 (2006).
27. X. M. Hu, G. L. Cheng, J. H. Zhou, X. Li, and D. Dan, Opt. Commun. **249,** 543 (2005).
28. V. Yannopapas, J. Phys. **18,** 6883 (2006).
29. X. M. Su, H. X. Kang, J. Kou, X. Z. Guo, and J. Y. Gao, Phys. Rev. A **80,** 023805 (2009).
30. H. J. Guo, Y. P. Niu, L. C. Wang, S. Q. Jin, and S. Q. Gong, Chin. Phys. Lett. **25,** 3656 (2008).